Available online at www.sciencedirect.com
ScienceDirect
Trans. Nonferrous Met. Soc. China 35(2025) 4184−4196
Transactions of Nonferrous Metals Society of China
www.tnmsc.cn

Effect of milling time on microstructure evolution and tribological properties of TiB_2−graphite hybrid reinforced Cu matrix composites

Heng-qing LI[1#], Jun-ming LU[1#], Yi-min GAO[2], Sheng-feng ZHOU[1], Bai-song GUO[1], Yi-ran WANG[2], Wei LI[1], Yang-zhen LIU[1,2,3]

1. Institute of Advance Wear & Corrosion Resistant and Functional Materials, College of Chemistry and Materials Science, Jinan University, Guangzhou 510632, China;
2. State Key Laboratory for Mechanical Behavior of Materials, Xi'an Jiaotong University, Xi'an 710049, China;
3. Shaoguan Research Institute of Jinan University, Shaoguan 512027, China

Received 1 March 2024; accepted 20 September 2024

Abstract: The effect of milling time on the microstructure and tribological properties of TiB_2−graphite hybrid reinforced Cu matrix composites was investigated. Hot-press sintering method was used to prepare the composites with different milling time (4, 6, 8, 10 and 12 h), and the tribological behaviors were studied. The results revealed that the relative density and electric conductivity of the composites initially increased and then decreased with an increase in milling time. The composites fabricated by milling for 6 h had the highest relative density and electric conductivity, which are 99.1% and 42.8%(IACS), respectively. The friction coefficient and wear rate of the composites initially decreased and then increased with an increase in milling time. The lowest friction coefficient and wear rate were measured to be 0.234 and 1.974×10^{-5} $mm^3/(N\cdot m)$, respectively, for the composites synthesized after 6 h of milling. The primary wear mechanism of the composites milled for 6 h was abrasive wear.

Key words: metal matrix composite; wear mechanism; milling time; hot-press sintering; tribological properties

1 Introduction

Copper (Cu) alloys have high electrical and thermal conductivities, good corrosion resistance and processing properties, which are widely used in power switches, brushes, bearings, and pantograph slides [1−4]. With the rapid development of power transmission, aerospace, rail transit and other fields, copper alloys must exhibit superior mechanical properties, electrical conductivities, and tribological behaviors. Some studies have shown that composites are an effective way to achieve the co-improvement in the structural and functional properties of copper materials [5−7]. Ceramic particles such as SiC, TiB_2, Al_2O_3, B_4C, TiC, and WC are commonly used as reinforcement phases in Cu-matrix composites [8−12]. Titanium diboride (TiB_2) is regarded as a good reinforcement phase because of its high hardness (25−34 GPa) and high elastic modulus (510−575 GPa) [13,14]. Although particle-reinforced Cu-matrix composites can effectively enhance the mechanical and wear properties of Cu-matrix composites, this is often at the expense of electrical conductivity. For example, JIANG et al [15] prepared in situ TiB_2(–TiB)/Cu composites using hot-pressing sintering, and the results showed that the strength of the composites increased, but the conductivity decreased significantly. SHI et al [16] and JHA et al [17] carried

# Heng-qing LI and Jun-ming LU contributed equally to this work
Corresponding author: Sheng-feng ZHOU, Tel/Fax: +86-20-85220890, E-mail: zhousf1228@163.com; Yang-zhen LIU, Tel/Fax: +86-20-85220890, E-mail: yangzhenliu@jnu.edu.cn
https://doi.org/10.1016/S1003-6326(25)66937-8

out studies on Al_2O_3- and TiN-reinforced metal matrix composites, respectively, and found that single particle reinforcement can improve the high-temperature softening resistance and wear resistance of the composites, but the electrical conductivity was not improved simultaneously. Therefore, solving the consistency problem among the strength, conductivity, and wear resistance of the composite has become the focus of research.

The design concept of multi-phase hybrid reinforced metal matrix composites is expected to achieve unity of strength, conductivity, and wear resistance [18,19]. Graphite can be considered a good secondary reinforcement phase because it not only has excellent electrical and thermal conductivities, but also is a good self-lubricating phase. Experimental studies revealed that the hybrid Cu/TiC–Gr composite has a lower friction coefficient and wear rate than the Cu/TiC composite [20]. Similarly, compared to CNTs/Cu and Al_2O_3/Cu, Cu/CNTs–Al_2O_3 reinforced Cu matrix composites have better mechanical properties and electrical conductivity [21]. FAYOMI et al [22], and SINGH and GAUTAM [23] revealed that hybrid-reinforced metal matrix composites can effectively improve comprehensive properties. Based on the above analysis, TiB_2−graphite hybrid reinforced Cu matrix composites are expected to have better comprehensive properties.

Powder metallurgy is commonly used to prepare TiB_2–graphite hybrid reinforced Cu matrix composites [24,25]. In powder metallurgy, milling time is an important factor affecting the properties of composites. For example, CHEN et al [26] studied the mechanical properties of high-entropy alloy reinforced Al matrix composites at different milling time and indicated that the average ultimate tensile strength and fracture strain of the composites were the poorest at a milling time of 20 h. OLIVEIRA et al [27] suggested that the crystallite size, microstrain, and lattice constants of Cu−5wt.% graphite composites were significantly correlated with milling time. Therefore, a suitable milling time can improve the comprehensive properties of TiB_2–graphite hybrid reinforced Cu matrix composites.

To date, there have been some reports on the properties of Cu matrix composites at different milling time, but most of these have mainly focused on mechanical properties [28−31], and the friction and wear properties have less been studied. Thus, there is a clear understanding of the interaction mechanism of the preparation process on the mechanical properties, but the relationship between milling time and wear mechanism of TiB_2–graphite hybrid reinforced Cu matrix composites is not clear. The tribological properties of bearings, brushes, and other parts are important evaluation indices. Therefore, it is very important to study the tribological behavior of TiB_2–graphite hybrid reinforced Cu matrix composites at different milling time.

In this study, the microstructural evolution of TiB_2–graphite hybrid reinforced Cu matrix composites at different milling time (4, 6, 8, 10 and 12 h) was estimated. The friction coefficients and wear rates of the composites at different milling time were investigated. The characteristics of the worn surface were observed, and the wear mechanism was analyzed.

2 Experimental

2.1 Materials

Three raw materials were used: electrolytic Cu powder (purity >99.9%, 45 μm, Luohong Metal Co., Ltd., China), graphite (purity >99.95%, 45 μm, Luohong Metal Co., Ltd., China), and TiB_2 powder (purity >99.99%, 50 μm, Luohong Metal Co., Ltd., China). The detailed morphologies of the raw materials are shown in Fig. 1. Owing to the poor wettability of graphite and TiB_2 with Cu, electroless copper plating on the surface of graphite and TiB_2 was used to improve their bonding properties. The plating process was divided into two steps: pre-treatment and electroless copper plating. Pre-treatment included cleaning, sensitization, and activation. The specific technological process was as follows: Firstly, flake graphite and TiB_2 were placed in 20 wt.% NaOH aqueous solution and boiled for 20 min in a horse boiler to remove the impurities on the surface of the graphite and TiB_2. Next, the pre-cleaned graphite and TiB_2 were sensitized in a mixture of 3 wt.% $SnCl_2$ and 5 wt.% HCl solution for 15 min, and then activated in a mixture of 5 wt.% HCl and 0.5 wt.% $PbCl_2$ solution for 10 min; the temperature of sensitization and activation was maintained at 40 °C. Finally, electroless copper plating of graphite and TiB_2 was completed within 60 min by electromagnetic agitation in the chemical solution with pH 12 and

60 °C. The chemical plating consisted of 16 wt.% copper sulfate pentahydrate ($CuSO_4·5H_2O$), 2 wt.% sodium hypophosphate ($NaH_2PO_2·H_2O$), and 1.5 wt.% sodium citrate ($C_6H_5Na_3O_7$). After vacuum filtration, Cu-coated graphite and TiB_2 were obtained; their morphologies are shown in Fig. 1. It can be seen that the coating thickness of Cu layer on the TiB_2 and graphite powders is 2.1 and 1.8 μm, respectively.

Cu-coated graphite, Cu-coated TiB_2, and Cu powders were prepared with a mass ratio of 7:5:88 and placed in a QM−BP planetary ball mill for 4, 6, 8, 10 and 12 h at 300 r/min. The ball-to-powder mass ratio was 5:1. The ground powders were poured into a graphite mold and placed in a rapid hot-pressing sintering furnace (FHP−828, China) under vacuum to obtain a cylindrical specimen with a diameter of 40 mm and a height of 10 mm. The sintering temperature was 800 °C, the holding period was 0.5 h, and the axial pressure was 30 MPa. Figure 2 describes a schematic diagram of the specimen preparation process.

2.2 Tests and characterization

The tribological properties (friction coefficient and wear rate) of the composites at different milling time were analyzed using the ball-on-disk reciprocating sliding mode on an MFT5000 tribometer (Rtec, USA). Disk specimens were composites with dimensions of 20 mm × 10 mm × 10 mm, the

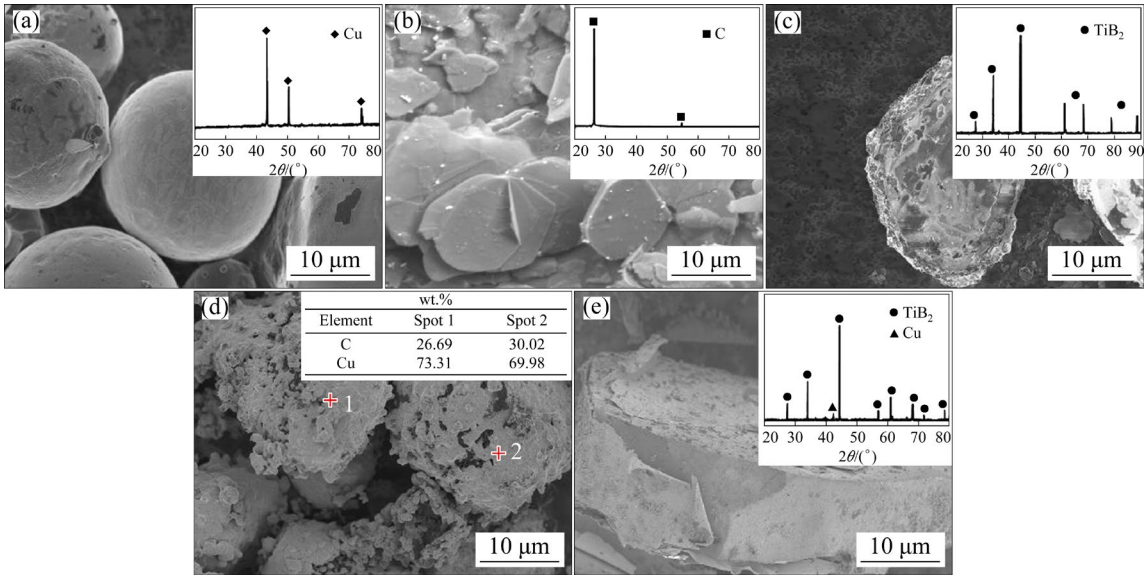

Fig. 1 Morphology of powders: (a) Raw copper powders; (b) Raw flake graphite; (c) Raw TiB_2; (d) Copper-coated graphite; (e) Copper-coated TiB_2

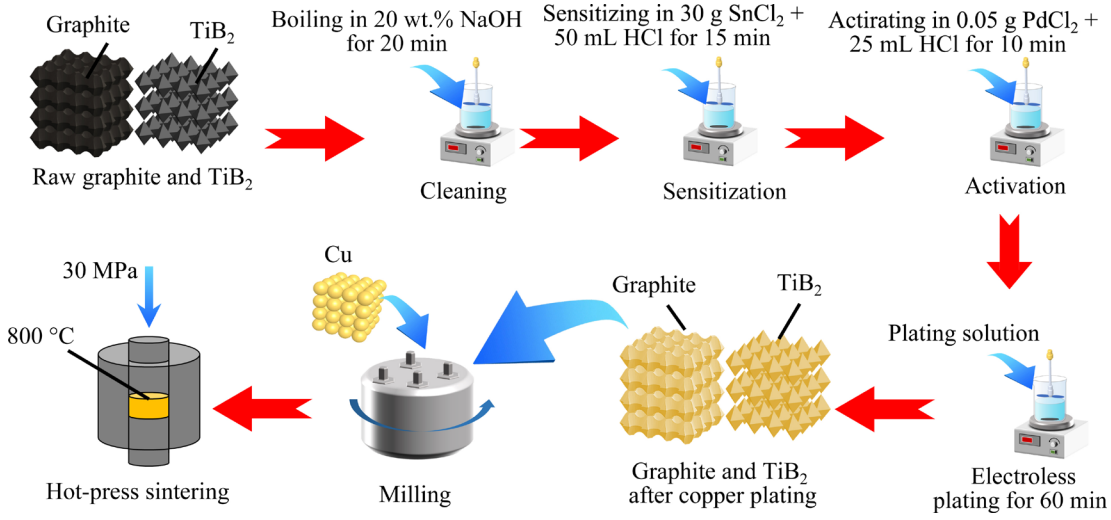

Fig. 2 Schematic diagram of specimen preparation

ball specimens were GCr15. The sliding distance, speed, and applied load were 100 m, 0.1 m/s, and 9 N, respectively. The friction coefficient was displayed on a computer in real-time during the experiment. Each specimen was tested at least three times to ensure data authenticity. Before each test, the surface of the specimen was polished and ultrasonically cleaned to roughness of $R_a \leq 0.1$ μm. The wear rate of the composite disks was calculated in a similar manner to the method of MIAO et al [32].

The actual densities of the composites were measured using the Archimedes method, and the relative densities were obtained. The formula is as follows:

$$\rho = \frac{1}{\frac{w(\mathrm{Cu})}{\rho_0(\mathrm{Cu})} + \frac{w(\mathrm{C})}{\rho_0(\mathrm{C})} + \frac{w(\mathrm{TiB_2})}{\rho_0(\mathrm{TiB_2})}} \times 100\% \quad (1)$$

where ρ is the relative density of the composite; w(Cu), w(C) and w(TiB$_2$) are the mass fractions of Cu, Cu-coated graphite and Cu-coated TiB$_2$ respectively; ρ_0(Cu), ρ_0(C) and ρ_0(TiB$_2$) are the actual densities of Cu, Cu-coated graphite and Cu-coated TiB$_2$, respectively. The Vickers hardness of the composites was estimated using an HXD−1000TMSC/LCD (Shanghai Wujiu Equipment Co., Ltd., China), and the average value of each composite after measuring ten points under a load of 0.098 N for 10 s was presented. A PZ−60A digital conductivity meter was used to estimate the electrical conductivity of the composites. To ensure the reliability of the results, five points were randomly selected on each surface for measurement.

By using the Image J, a free image processing software, the dimensions of the powder particles at different milling time were analyzed using scanning electron microscopy (SEM). To ensure the reliability of the results, at least 100 images were counted, and the average value was obtained. SEM was used to observe the microstructural evolution of the composites and characterize the worn surfaces (disk, ball and wear products). A 3D laser-scanning profilometer was used to analyze the three-dimensional (3D) structure of the disk worn surface. X-ray diffraction (XRD) was performed to investigate the phase composition of the composites. Energy dispersive spectroscopy (EDS) and X-ray photoelectron spectroscopy (XPS) were used to characterize the element composition and bonding type of the worn surfaces.

3 Results and discussion

3.1 Microstructure and properties of composites

Figure 3 presents SEM images of the composite powders at different milling time. Due to the severe deformation, cold welding, and crushing of the powders during the milling process, the morphology, size, and distribution of the powders have changed significantly. Therefore, the sizes of the powders decreased with an increase in milling time, and the average particle sizes of the powders at milling time of 4, 6, 8, 10 and 12 h were 25.60, 19.50, 9.42, 9.23 and 5.90 μm respectively. In

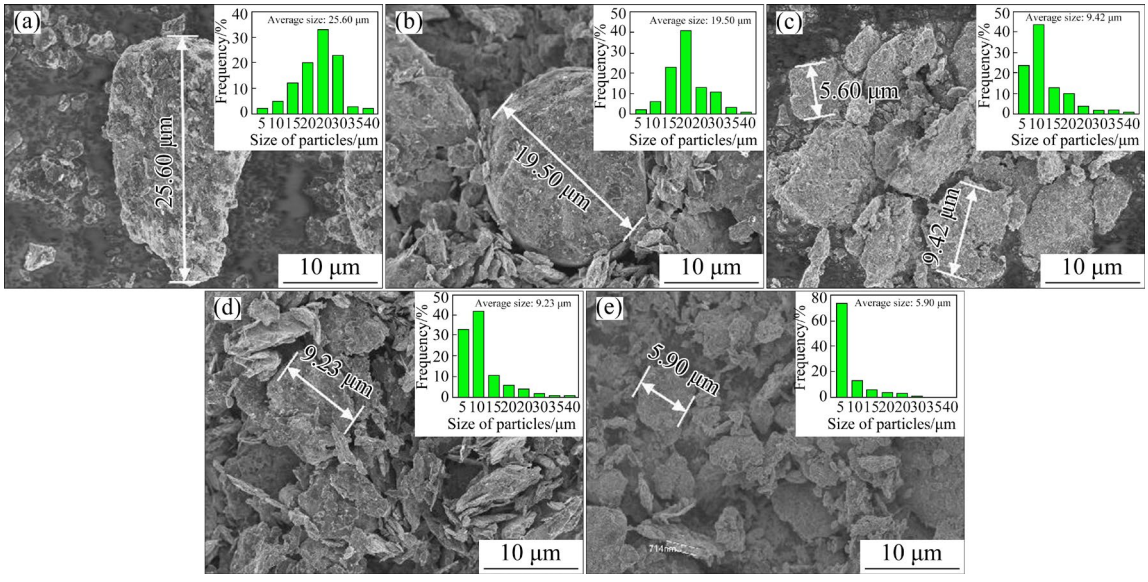

Fig. 3 SEM images of composite powders at different milling time: (a) 4 h; (b) 6 h; (c) 8 h; (d) 10 h; (e) 12 h

addition, the size distribution of the composite powder particles tended to be uniform with an increase in milling time. When the milling time reached 4 h (Fig. 3(a)), the morphology of a significant amount of the powders changed to irregular morphology, but some powders still retained a spherical morphology. With further increasing milling time to 6 h, it was almost impossible to observe isolated single-phase particles, and the phase compositions of these particles could not be distinguished. More and more powders transformed into the flake form (Fig. 3(b)). However, long-term shearing and cold welding resulted in a decrease in the ductility of the composite powders, more serious particle fracture, and a more superfine flake-like morphology of the powder particles, as shown in Figs. 3(c−e). Therefore, the particle shape changed from spherical to flake during the early milling stage, and the shape of the composite powders became superfine flake-like structure with a further increase in milling time. It can also be said that the homogeneous distribution and morphological characteristics of the particles play a crucial role in the properties of the composites as found in previous study [33].

Figure 4 displays the XRD patterns of the composites prepared at different milling time. Only the diffraction peaks of C, TiB_2 and Cu were observed, indicating that no chemical reaction occurred between the components throughout the powder metallurgy preparation process, and that the (C−TiB_2)/Cu composites were successfully synthesized. The intensity of each diffraction peak decreased with increasing milling time; in particular, when the milling time exceeded 8 h, the peaks of C and TiB_2 basically disappeared. This indicated that the crystallite size was below the XRD detection limit. In addition, the full width at half maximum (FWHM) steadily increased with increasing milling time. The main reason for this was that there were more defects and stresses in the powders, and the crystal structure was destroyed during the milling process, resulting in a decrease in the grain size and serious lattice distortion [34,35].

Figure 5 reveals the microstructures of the composites perpendicular to the hot-pressing direction at different milling time. The dimensions of the powders remained large when the milling time was short, and there was little difference in the raw powder morphology (Fig. 5(a)). The morphology of the particles became flatter, the size decreased, and the dispersion became more uniform with a further increase in the milling time (6 and 8 h, Figs. 5(b, c)). As the milling time was further increased to 10 or 12 h (Figs. 5(d, e)), although the size of the particles was further reduced, there was clear agglomeration between the particles, and the splitting effect of the Cu matrix was also significant, which inevitably influenced the properties of the composites.

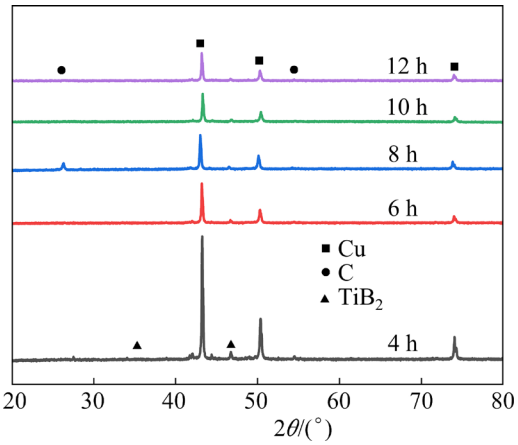

Fig. 4 XRD patterns of Cu matrix composites at different milling time

The physical and mechanical properties such as relative density, electrical conductivity, porosity and hardness of (C−TiB_2)/Cu composites at different milling time are listed in Table 1. It is worth noting that the hardness of the composite increased with increasing milling time and was greater than that of pure copper (HV 86.5 [36]) at milling time higher than 6 h. On the one hand, the hardness increased owing to the effect of fine-grained strengthening. However, when the indenter underwent plastic deformation on the surface of the composite, the TiB_2 particles effectively prevented the slipping of dislocations and grain boundaries in the matrix and improved the hardness.

The relative density of the composites initially increased and then decreased with increasing milling time, and the maximum value appeared at 6 h. When the milling time was short, the Cu powders transformed from spherical shape to flake-like shape (Figs. 5(a, b)), which effectively reduced the porosity at the interface and promoted uniform settlement of the reinforced phase at the phase boundary. Similar results have also been explained

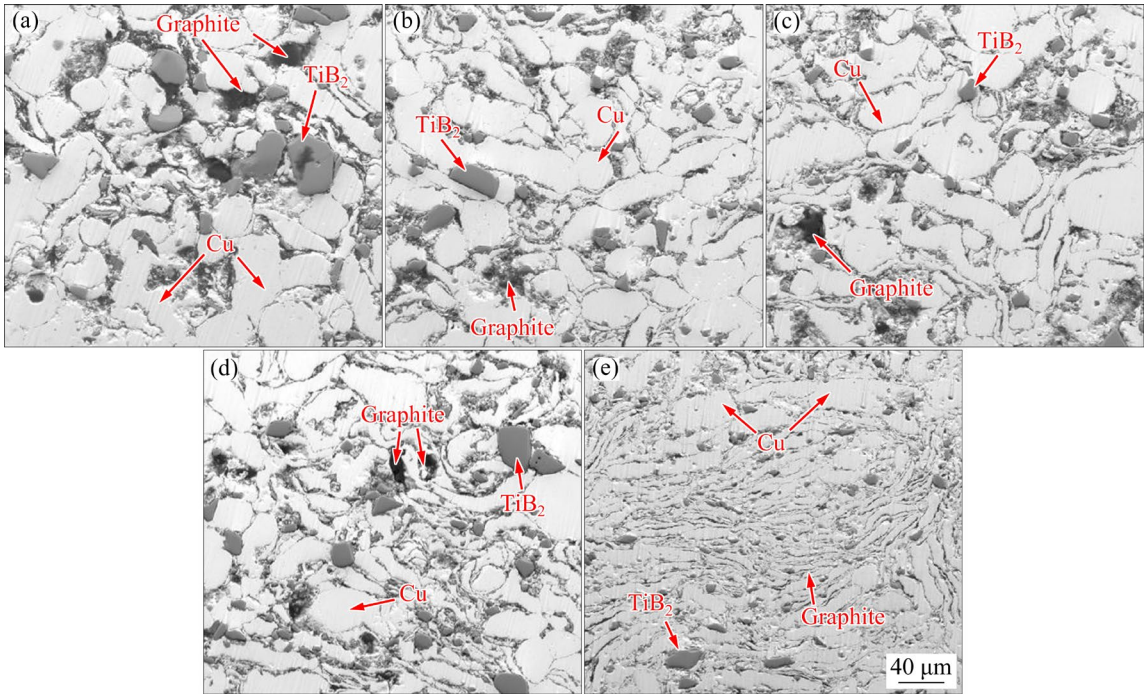

Fig. 5 Microstructures of composites at different milling time: (a) 4 h; (b) 6 h; (c) 8 h; (d) 10 h; (e) 12 h

Table 1 Physical and mechanical properties of composites at different milling time

Milling time/h	Hardness (HV)	Relative density/%	Porosity/%	Electrical conductivity/%(IACS)
4	84.8±2.9	91.8±0.4	8.3±0.5	19.8±0.7
6	88.4±1.9	99.1±0.3	0.8±0.2	42.8±0.8
8	89.1±2.3	95.7±0.6	4.5±0.4	25.2±0.4
10	90.3±3.0	94.1±0.3	5.9±0.3	21.2±0.6
12	92.8±2.4	92.3±0.5	7.6±0.6	20.4±0.6

in other studies [37]. The dimensions of the particles decreased gradually with increasing milling time; however, the interfacial area between various fine particles increased, resulting in an increase in interfacial porosity and a decrease in density.

For electrical conductivity, it also initially increased and then decreased with an increase in milling time, and reached the maximum value at 6 h (42.8%(IACS)). One of the reasons for the electrical conductivity change was that the flake morphology of the powders after copper plating facilitated the uniform distribution of the particles in the Cu matrix (Fig. 5(b)). On the other hand, it can be observed that there were Cu regions deposits around the grains. With further increasing milling time, the grain size became smaller and the grain boundary increased, which improved the ability of electron flow and led to the decrease of electrical conductivity.

3.2 Tribological properties

Figure 6 shows the tribological properties (friction coefficient and wear rate) of the composites at various milling time. As shown in Fig. 6(a), the friction coefficient initially decreased and then increased with increasing milling time, with the lowest value appearing at 6 h (0.234). A possible reason for this was that the reinforcing phase size was large and the embedding matrix was incomplete when the milling time was short (Fig. 5(a)), resulting in the distribution of agglomerated graphite at the wear interface, and the tribofilm was not completely formed; the TiB_2 particles prevented the movement of the grinding ball on the friction surface and increased the friction coefficient. When the milling time was extended to 6 h, the distribution of the TiB_2 and graphite particles in the Cu matrix was more uniform than

that at 4 h (Fig. 5(b)). This was also conducive to the formation of a uniform lubricating film on the surface of the composites, which reduced the friction coefficient. However, with a further increase in the milling time, the graphite and TiB_2 particles were broken after impact for a long time, and the particle agglomeration was significant, which caused poor interface bonding, severe particle drop, and the integrity and continuity of the lubrication film could not be guaranteed, resulting in an increase in the friction coefficient.

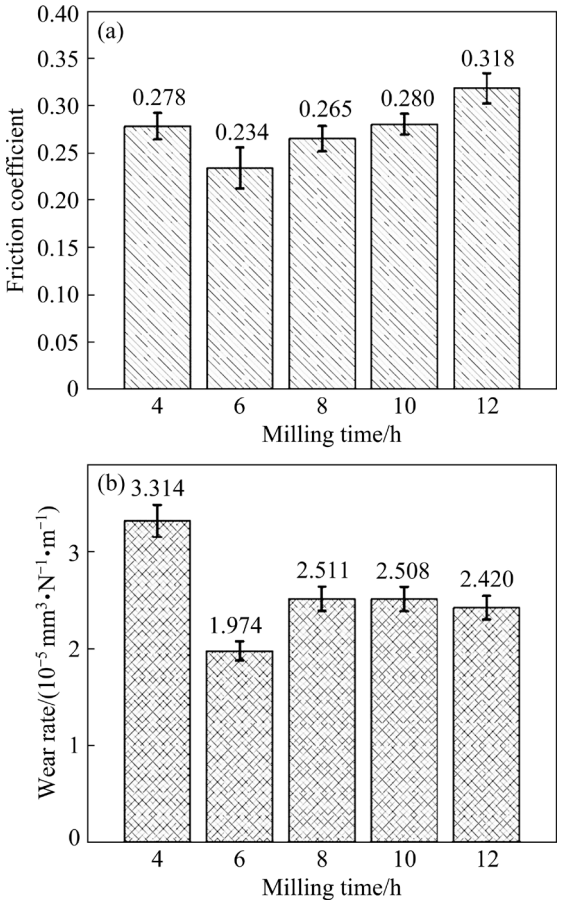

Fig. 6 Tribological properties of composites at different milling time: (a) Friction coefficient; (b) Wear rate

From Fig. 6(b), the wear rate initially decreased and then increased with increasing milling time, similar to the changes in the friction coefficient. The lowest wear rate of the composites was observed at a milling time of 6 h. At this time, the wear rate decreased by 40.4% compared with that at a milling time of 4 h. The main reason for this was that the particle distribution was more uniform at 6 h (Fig. 5(b)), but the actual contact area between the dual-ball and the composite was also reduced with an increase in the hardness of the composites (Table 1), which prevented the reinforced phases from falling off easily, and the surface was more conducive to the formation of the lubricating film. When the milling time exceeded 6 h, the wear rate of the composites increased further. This was mainly because the dimensions of the particles decreased, the interface area increased, the porosity increased, and particle agglomeration intensified, resulting in further spalling of the particles during the friction process. In addition, the interfacial bond between the reinforced phases and Cu was weak, and the graphite and TiB_2 phases were extruded into the tribo-pair during the reciprocating sliding process, resulting in three-body wear. The surface area of the composites and wear rate increased.

3.3 Worn surfaces and wear mechanism

To understand the tribological behavior of the composites at different milling time, the 3D profiles and roughness R_a of the wear scars were analyzed, as shown in Fig. 7. The results revealed that the width and roughness of the wear scars initially decreased and then increased with increasing the milling time. The wear scars at 6 h had the smallest width and roughness of (950.32±39.75) μm and (241.04±13.86) nm, respectively. This was mainly due to the uniform dispersion of the reinforcement particles and the formation of surface lubrication film. Therefore, compared with those at 12 h, the width and roughness of the wear scars at 6 h were reduced by 21.1% and 19.1%, respectively, which was consistent with the tribological behavior analyzed above (Fig. 6(b)).

The SEM images of the worn surfaces, dual-balls, and wear debris of the composites at different milling time are shown in Fig. 8. The worn surface of the composite had more pitting corrosion, more furrows, and clear peeling at 4 h (Fig. 8(a)), while the dual-ball also showed significant furrows and peeling (Fig. 8(a1)), similar to the composite worn surface. This was precisely due to the greater roughness of the worn surface, where the size of the wear debris was larger (Fig. 8(a2)). Therefore, the wear mechanism was fatigue wear. When the milling time increased to 6 h, the worn surface was the smoothest; only a few shallow furrows were observed (Fig. 8(b)) and a uniform tribofilm was formed on the dual-ball surface (Fig. 8(b1)). As the wear surface had a good tribofilm, it had good

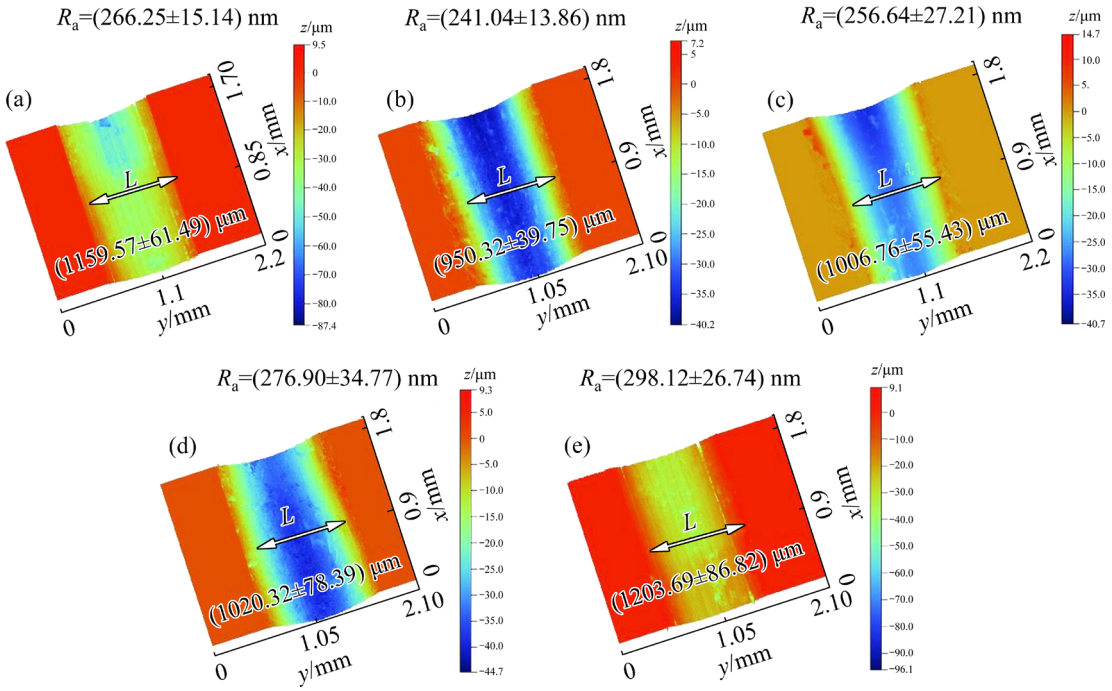

Fig. 7 3D profile and roughness of wear scars perpendicular to sliding directions of composites at different milling time: (a) 4 h; (b) 6 h; (c) 8 h; (d) 10 h; (e) 12 h

tribological properties, which was consistent with the previous analysis of the wear rate. Consequently, it exhibited less wear debris (Fig. 8(b2)). Subsequently, abrasive wear was dominant at 6 h. In addition, numerous pits and small amounts of peeling appeared on the surface of the composite after 8 h (Fig. 8(c)). There were significant deep furrows and adhesion of tribo-products on the dual-ball surface (Fig. 8(c1)). Therefore, the size of the wear debris at this time was larger than that at 6 h (Fig. 8(c2)). The results revealed that the primary wear mechanism was oxidative. With a further increase in the milling time to 10 and 12 h, large-scale peeling of the worn surface occurred, broken graphite-phase particles could also be observed (Figs. 8(d, e)), and the dual-ball surface adhered to a large number of tribo-products (Figs. 8(d1, e1)). Meanwhile, the size of the wear debris was too large because of the large-scale peeling of the reinforced phase (Figs. 8(d2, e2)). Thus, the adhesive wear was dominant.

To further explain the wear mechanism of the composites, EDS analysis was conducted on the points of the composite worn surfaces and dual-balls identified by the capital letters, as listed in Table 2. C, O, Fe, Cu, and Ti were observed on both the composite worn surfaces and the dual-balls, indicating that oxidation occurred during the reciprocating sliding process. The O content on the composite surface initially increased and then decreased, whereas the Fe and Cu contents initially decreased and then increased with increasing milling time. A possible explanation was that a tribofilm was formed on the worn surface when the milling time was short, and the tribofilm was peeled off owing to the agglomeration of the reinforcing phase with increasing milling time, leaving the matrix exposed. Together, the oxidation and lubrication films formed a tribofilm on the surface. Moreover, the composition of the dual-ball surface was similar to that of the tribofilm generated by the composite surface, which revealed that the formation of the dual-ball surface may be due to the transfer of tribo-products onto the composite surface. In particular, it should be noted that only C, O, Fe, and extremely small amounts of Cu were detected on the dual-ball surface at a milling time of 6 h, suggesting that only small or even negligible amounts of products were transferred from the composite surface. The Cu content on the dual-ball surfaces initially decreased and then increased with increasing milling time, which indicated that the effect of adhesive wear initially decreased and then increased with increasing milling time.

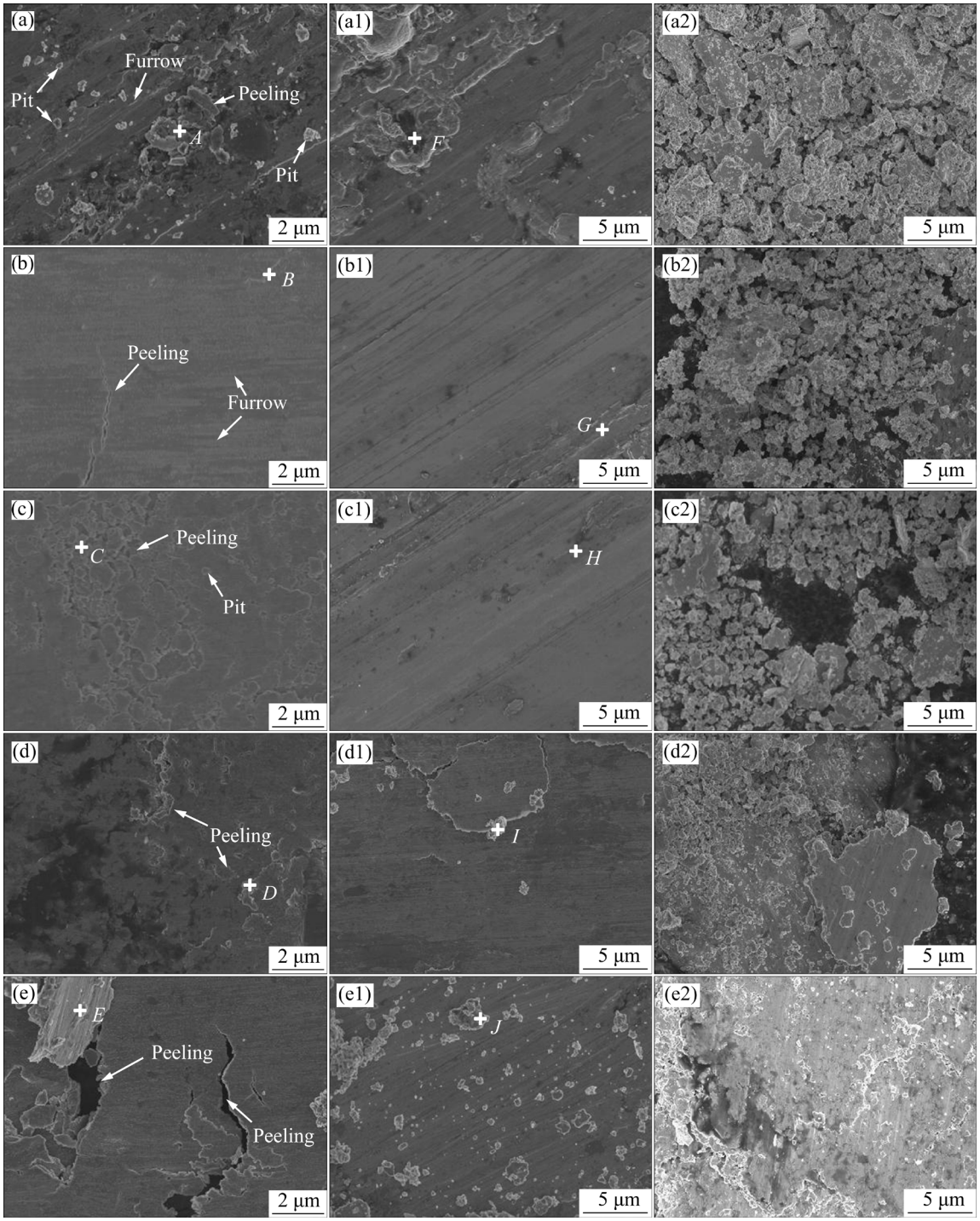

Fig. 8 SEM images of worn surface (a−e), dual-balls (a1−e1), and wear debris (a2−e2) of composites at different milling time: (a, a1, a2) 4 h; (b, b1, b2) 6 h; (c, c1, c2) 8 h; (d, d1, d2) 10 h; (e, e1, e2) 12 h

To determine the lubrication mechanism of the composite and the chemical bond composition of the tribofilm at a milling time of 6 h, the chemical composition of the tribofilm was analyzed using XPS. After the back and bottom were removed, the fine spectrum of each element was fitted using the Avantage software, as shown in Fig. 9. For the fine spectrum of C 1s (Fig. 9(a)), the peaks at 284.8 and 286.5 eV were attributed to C—C and C—O—C of graphite, respectively, while the peak near 288.3 eV was derived from C═O of the graphite [38], which indicated that graphite was involved in the formation of tribofilm. The fine spectrum of Cu 2p consisted of four peaks (Fig. 9(b)): the peaks

Table 2 Element contents of various points in Fig. 8 on worn surfaces and dual-balls (at.%)

Element	*A*	*B*	*C*	*D*	*E*	*F*	*G*	*H*	*I*	*J*
C	20.27	25.21	21.47	23.41	26.85	23.37	22.89	20.04	26.22	21.31
O	30.25	33.67	30.31	28.64	18.48	58.86	58.52	59.34	50.19	54.73
Fe	6.88	5.17	5.79	6.41	6.9	15.49	18.29	18.01	16.31	11.25
Cu	39.53	34.96	39.34	40.09	45.55	2.07	0.3	2.5	7.11	8.39
Ti	3.07	0.99	3.09	1.45	2.22	0.21	0	0.11	0.17	4.32

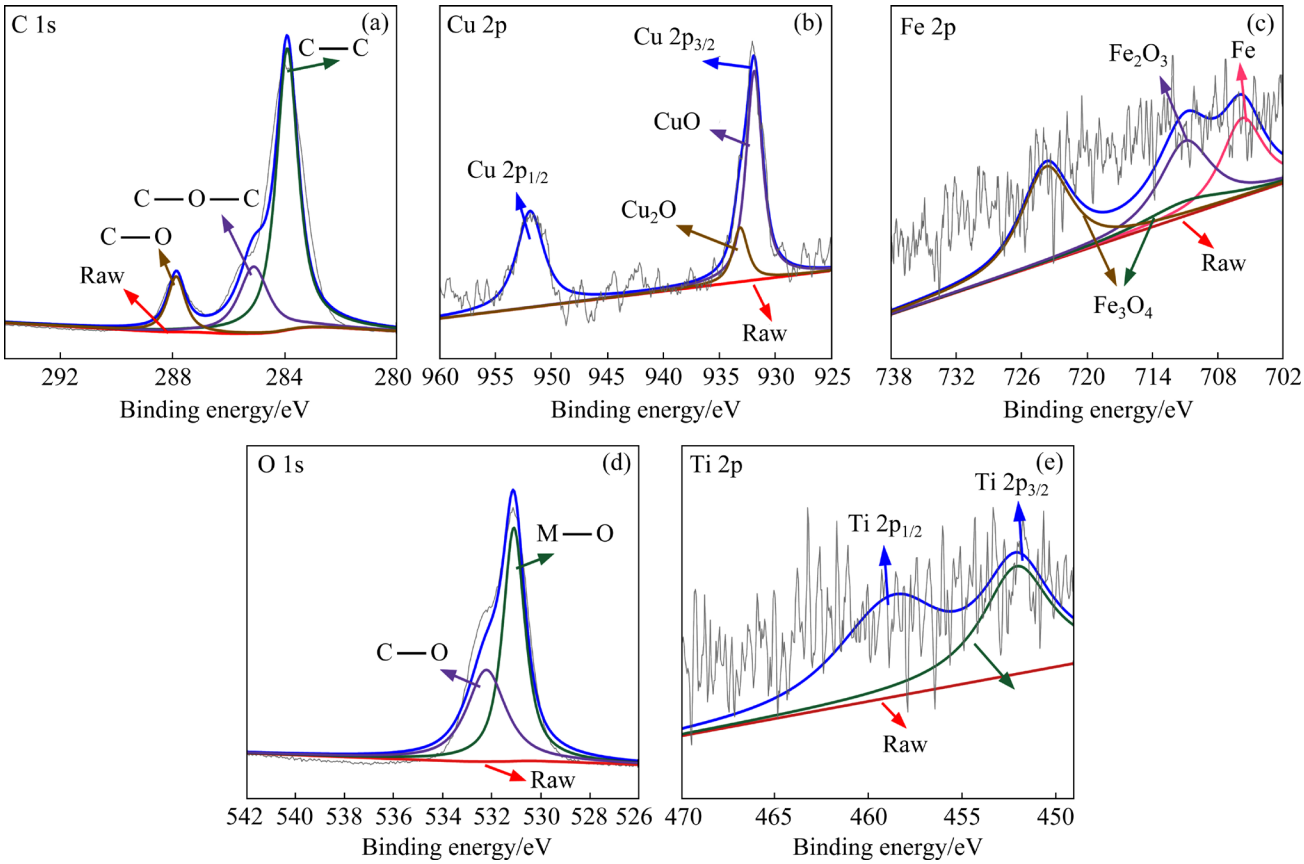

Fig. 9 Worn surface XPS spectra of composite at milling time of 6 h

located around 931.3 eV (CuO) and 932.6 eV (Cu_2O) belonged to the Cu—O species, and the other peaks near 930.8 and 951.3 eV demonstrated the existence of Cu. In terms of the fine spectra of Fe 2p, the characteristic peaks of Fe (705.8 eV [39]), Fe_2O_3 (711.3 eV [40]) and Fe_3O_4 (709.2 eV [41]) were obtained (Fig. 9(c)). The results show that there was material transfer between the composite and dual-balls during the sliding process, which indirectly confirmed the occurrence of adhesive wear. This demonstrated that the agreement between this phenomenon and the distribution of elements on the worn surface was quite good. From the fine spectrum of O 1s, the peak near 530.6 eV was proven to be a metal oxide, which not only indicated the occurrence of oxidative wear, but also showed the existence of an oxide film in the tribofilm (Fig. 9(d)). Ti 2p exhibited three peaks (Fig. 9(e)), of which the characteristic peaks near 451.8 and 458.4 eV were attributed to Ti, and the peak at 450.9 eV belonged to TiO_2. Therefore, the tribofilm mainly consisted of a Cu matrix, graphite, CuO, Cu_2O, Fe, Fe_2O_3, Fe_3O_4 and TiO_2. Several studies have reported relevant lubrication mechanisms. One of the main reasons is that dual role of the formation of oxidation and lubrication films on the composite surface can effectively increase the wear resistance and reduce the friction coefficient [42−44].

4 Conclusions

(1) Only C, TiB_2 and Cu were observed in the XRD patterns, indicating that no chemical reaction occurred between the powders at different milling time. The particle size of the powder decreased with increasing milling time. It can be seen that the copper plating reinforcement phase was more homogeneously distributed in the Cu matrix at 6 h, which played a crucial role in improving the wear rate and electrical conductivity of the composites.

(2) The relative density and electrical conductivity of the composites initially increased and then decreased with increasing milling time. Samples with the highest relative density (about 99.1%) and electrical conductivity (about 42.8%(IACS)) were found at a milling time of 6 h. The hardness of the composites increased with increasing milling time, and it was HV 84.8, HV 88.4, HV 89.1, HV 90.3 and HV 92.8 at milling time of 4, 6, 8, 10 and 12 h, respectively.

(3) The friction coefficient and wear rate of the composites initially decreased and then increased with increasing milling time, with the lowest values appearing at 6 h (0.234 and 1.974×10^{-5} $mm^3/(N\cdot m)$, respectively). The composites with excellent comprehensive properties were achieved at milling time of 6 h. The primary wear mechanism of the composites after milling for 6 h was abrasive wear.

CRediT authorship contribution statement

Heng-qing LI: Methodology, Data curation, Investigation, Writing − Original draft; **Jun-ming LU:** Data curation, Investigation; **Yi-min GAO:** Funding acquisition; **Sheng-feng ZHOU:** Formal analysis, Conceptualization; **Bai-song GUO:** Data curation, Validation; **Yi-ran WANG:** Visualization, Validation; **Wei LI:** Methodology, Supervision; **Yang-zhen LIU:** Supervision, Resources, Formal analysis, Conceptualization, Writing − Review & editing.

Declaration of competing interest

The authors declare that they have no known competing financial interests or personal relationships that could have appeared to influence the work reported in this paper.

Acknowledgments

The authors would like to thank the financial support from the Fundamental Research Funds for the Central Universities, China (Nos. 21623416, 21622110), the Science and Technology Research Program of Guangzhou, China (No. 2024A04J3963), the National Natural Science Foundation of China (Nos. 52271132, 52373236, 92166112), the Guangdong Basic and Applied Basic Research Foundation, China (Nos. 2020A1515111067, 2021A1515010890, 2023A1515012850, 2020B1515420004), and the Open Fund of State Key Laboratory for Mechanical Behavior of Materials, Xi'an Jiaotong University, China (No. 20222410).

References

[1] LI H, NIU D T, ZHANG Z T, YANG F, WANG H X, CHENG W L. Tailoring microstructure, mechanical and wear properties of Mn_5Si_3 reinforced Cu−35Zn−3Al alloy via melt superheat combined with pulsed magnetic field [J]. Transactions of Nonferrous Metals Society of China, 2024, 34: 918−934.

[2] QIN Y Q, ZHUANG Y, LUO L M, ZHANG Y F, WU Y C. Effect of alloying element Zr on microstructure and properties of Cu−Y_2O_3 composites [J]. Transactions of Nonferrous Metals Society of China, 2023, 33: 3418−3426.

[3] LIU F X, LIU X H, XIE G L, WU Y, CHEN C G. Studies on thermal stability, softening behavior and mechanism of an ADS copper alloy at elevated temperatures [J]. Journal of Materials Science & Technology, 2024, 186: 79−90.

[4] ZHANG H T, FU H D, ZHU S C, YONG W, XIE J X. Machine learning assisted composition effective design for precipitation strengthened copper alloys [J]. Acta Materialia, 2021, 215: 117118.

[5] XIE Z N, GUO H, XIAO W, ZHANG X M, HUANG S H, SUN M M, XIE H F. Interfacial structures and their effect on thermal conductivity and mechanical properties of diamond/Cu−B composites [J]. Transactions of Nonferrous Metals Society of China, 2024, 34: 246−254.

[6] ZHU J M, LI J W, LIU T, CHEN Z, FANG H C, XIAO P, KONG F. Differences in mechanical behaviors and characteristics between natural graphite/copper composites and carbon-coated graphite/copper composites [J]. Materials Characterization, 2020, 162: 110195.

[7] ALI S, AHMAD F, YUSOFF P S M M, MUHAMAD N, OÑATE E, RAZA M R, MALIK K. A review of graphene reinforced Cu matrix composites for thermal management of smart electronics [J]. Composites (Part A): Applied Science and Manufacturing, 2021, 144: 106357.

[8] LI J Y, LÜ S L, CHEN L, LIAO Q, GUO W, WU S S. Influence of squeeze casting pressure on nanoparticle distribution and mechanical properties of nano-SiC_p/Al−Cu composites assisted with ultrasonic vibration [J]. Transactions of Nonferrous Metals Society of China, 2023, 33: 1977−1987.

[9] VAROL T, CANAKCI A, YALCIN E D. Fabrication of nanoSiC-reinforced Al2024 matrix composites by a novel production method [J]. Arabian Journal for Science and Engineering, 2017, 42: 1751−1764.

[10] VAROL T, GÜLER O, AKÇAY S B, AKSA H C. The effect of silver coated copper particle content on the properties of novel Cu−Ag alloys prepared by hot pressing method [J]. Powder Technology, 2021, 384: 236−246.

[11] WANG L, TIEU A K, ZHU Q, CHEN J, CHENG J, YANG J, KOSASIH B. Achieving the excellent self-lubricity and low wear of TiAl intermetallics through the addition of copper coated graphite [J]. Composites (Part B): Engineering, 2020, 198: 108223.

[12] CANAKCI A, VAROL T, ERTOK S. The effect of mechanical alloying on Al_2O_3 distribution and properties of Al_2O_3 particle reinforced Al-MMCs [J]. Science and Engineering of Composite Materials, 2012, 19: 227−235.

[13] WANG H, ZHANG H M, CUI Z S, CHEN Z, CHEN D. Ductile fracture behavior of in situ TiB_2 particle reinforced 7075 aluminum matrix composite in various stress states [J]. Transactions of Nonferrous Metals Society of China, 2023, 33: 2272−2286.

[14] CHEN X, WANG H T, JI G C, BAI X B, FU W. Microstructure and properties of TiB_2−Ni coatings with different binder phase contents deposited by HVOF spray process [J]. Rare Metals, 2022, 41: 1385−1393.

[15] JIANG Y H, WANG C, LIANG S H, REN J Q, DU X, LIU F. TiB_2(−TiB)/Cu in-situ composites prepared by hot-press with the sintering temperature just beneath the melting point of copper [J]. Materials Characterization, 2016, 121: 76−81.

[16] SHI Y G, CHEN W G, DONG L L, LI H Y, FU Y Q. Enhancing copper infiltration into alumina using spark plasma sintering to achieve high performance Al_2O_3/Cu composites [J]. Ceramics International, 2018, 44: 57−64.

[17] JHA P, GAUTAM R K, TYAGI R. Friction and wear behavior of Cu−4wt.%Ni−TiC composites under dry sliding conditions [J]. Friction, 2017, 5: 437−446.

[18] LIU S W, WU H J, XIE X L, JI G, MOLIERE M, LIAO H L. Tribological properties of cold-sprayed 7075Al coatings reinforced with hybrid nano-TiB_2/micro-SiC particles [J]. Surface and Coatings Technology, 2023, 458: 129323.

[19] JIANG X S, LIU W X, LI Y J, SHAO Z Y, LUO Z P, ZHU D G, ZHU M H. Microstructures and mechanical properties of Cu/Ti_3SiC_2/C/ graphene nanocomposites prepared by vacuum hot-pressing sintering and hot isostatic pressing [J]. Composites Part B: Engineering, 2018, 141: 203−213.

[20] MIRANDA-LÓPEZ A, LEÓN-PATIÑO C A, AGUILAR-REYES E A, BEDOLLA-BECERRIL E, RODRIGUEZ-ORTIZ G. Effect of graphite addition on wear behaviour of hybrid Cu/TiC−Gr infiltrated composites [J]. Wear, 2021, 484: 203793.

[21] CHEN F, MEI Q S, LI J Y, LI C L, WAN L, MEI X M, CHEN Z H, XU T, WANG Y C, TAN Y Y. Achieving synergistic strengthening and enhanced comprehensive properties of Cu matrix composites at high strength level by incorporating nanocarbons and Al_2O_3 dual reinforcements [J]. Materials Science and Engineering: A, 2022, 839: 142859.

[22] FAYOMI J, POPOOLA A P I, OLADIJO O P, POPOOLA O M, FAYOMI O S I. Experimental study of ZrB_2−Si_3N_4 on the microstructure, mechanical and electrical properties of high grade AA8011 metal matrix composites [J]. Journal of Alloys and Compounds, 2019, 790: 610−615.

[23] SINGH M K, GAUTAM R K. Structural, mechanical, and electrical behavior of ceramic-reinforced copper metal matrix hybrid composites [J]. Journal of Materials Engineering and Performance, 2019, 28: 886−899.

[24] LONG F, GUO X H, SONG K X, JIA S G, YAKUBOV V, LI S L, LIANG S H. Enhanced arc erosion resistance of TiB_2/Cu composites reinforced with the carbon nanotube network structure [J]. Materials & Design, 2019, 183: 108136.

[25] LONG F, GUO X H, SONG K X, JIA S G, YAKUBOV V, LI S L, YANG Y B, LIANG S H. Synergistic strengthening effect of carbon nanotubes (CNTs) and titanium diboride (TiB_2) microparticles on mechanical properties of copper matrix composites [J]. Journal of Materials Research and Technology, 2020, 9: 7989−8000.

[26] CHEN W P, LI Z X, LU T W, HE T B, LI R K, LI B, WAN B B, FU Z Q, SCUDINO S. Effect of ball milling on microstructure and mechanical properties of 6061Al matrix composites reinforced with high-entropy alloy particles [J]. Materials Science and Engineering: A, 2019, 762: 138116.

[27] OLIVEIRA E V, COSTA F A, RAIMUNDO R A, LOURENÇO C S, MORALES M A, MATHAUDHU S N, GOMES U U. Effect of milling time in characteristics of the powder Cu−5wt.%graphite [J]. Advanced Powder Technology, 2022, 33: 103360.

[28] WANG Y R, GAO Y M, LI Y F, ZHANG C, HUANG X Y, ZHAI W Y. Effect of milling time on microstructure and mechanical properties of Cu−Ni-graphite composites [J]. Materials Research Express, 2017, 4: 096506.

[29] SALUR E. Synergistic effect of ball milling time and nano-sized Y_2O_3 addition on hardening of Cu-based nanocomposites [J]. Archives of Civil and Mechanical Engineering, 2022, 22: 103.

[30] ABU-OQAIL A, WAGIH A, FATHY A, ELKADY O, KABEEL A M. Effect of high energy ball milling on strengthening of Cu−ZrO_2 nanocomposites [J]. Ceramics International, 2019, 45: 5866−5875.

[31] SORKHE Y A, AGHAJANI H, TAGHIZADEH TABRIZI A. Mechanical alloying and sintering of nanostructured TiO_2 reinforced copper composite and its characterization [J]. Materials & Design, 2014, 58: 168−174.

[32] MIAO J W, LIANG H, ZHANG A J, HE J Y, MENG J H, LU Y P. Tribological behavior of an AlCoCrFeNi2.1 eutectic high entropy alloy sliding against different counterfaces [J]. Tribology International, 2021, 153: 106599.

[33] GÜLER O, VAROL T, ALVER Ü, ÇANAKÇI A. The effect of flake-like morphology on the coating properties of silver coated copper particles fabricated by electroless plating [J]. Journal of Alloys and Compounds, 2019, 782: 679−688.

[34] LI C, PIAO Y C, MENG B B, HU Y X, LI L Q, ZHANG F H. Phase transition and plastic deformation mechanisms induced by self-rotating grinding of GaN single crystals [J]. International Journal of Machine Tools and Manufacture, 2022, 172: 103827.

[35] PANG Y P, LIU Y F, ZHANG X, GAO M X, PAN H G. Role of particle size, grain size, microstrain and lattice distortion in improved dehydrogenation properties of the ball-milled $Mg(AlH_4)_2$ [J]. International Journal of Hydrogen Energy, 2013, 38: 1460−1468.

[36] LI Z H, LIU L, YOU X, YI J H, BAO R, ZHU M Y, LU S, PAI J J. Cooperative enhancement of mechanical and tribological properties through tailoring TiN transition interface in boron nitride nanosheets reinforced copper composites [J]. Rare Metals, 2024, 43(10): 5202−5215.
[37] GÜLER O, VAROL T, ALVER Ü, CANAKCI A. Effect of Al_2O_3 content and milling time on the properties of silver coated Cu matrix composites fabricated by electroless plating and hot pressing [J]. Materials Today Communications, 2020, 24: 101153.
[38] GUAN Z P, WU Z C, LIU J, TU X H, LI S J. Controllable fabrication of magnesium silicate hydroxide reinforced MoS_2 hybrid nanomaterials as effective lubricant additives in PAO [J]. Applied Surface Science, 2022, 597: 153777.
[39] DI CASTRO V, CIAMPI S. XPS study of the growth and reactivity of Fe/MnO thin films [J]. Surface Science, 1995, 331/332/333: 294−299.
[40] MATTS O E, TARASOV S Y, DOMENICHINI B, LAZURENKO D V, FILIPPOV A V, BATAEV V A, RASHKOVETS M V, CHAKIN I K, EMURLAEV K I. Tribo-oxidation of Ti−Al−Fe and Ti−Al−Mn cladding layers obtained by non-vacuum electron beam treatment [J]. Surface and Coatings Technology, 2021, 421: 127442.
[41] XIAO G G, JIANG L, PENG W M, LIU J W, DENG C B, QIAN L M. Towards a deep understanding of oxidation in the material removal of GCr15 bearing steel during chemical mechanical polishing [J]. Wear, 2022, 508/509: 204466.
[42] WANG L G, TONG Y G, ZHOU C, LI Y J, LIU J, CAI Z H, WANG H D, HU Y L. Self-lubricating Ti_3SiC_2 strengthening Cu composites with electrical conductivity and wear resistance trade off [J]. Tribology International, 2023, 187: 108724.
[43] DINAHARAN I, ALBERT T. Effect of reinforcement type on microstructural evolution and wear performance of copper matrix composites via powder metallurgy [J]. Materials Today Communications, 2023, 34: 105250.
[44] WANG Y J, ZHAO X Q, HAO E K, BU Z Y, AN Y L, ZHOU H D, CHEN J M. High temperature induced “glaze” layer formed in HVOF-sprayed NiCrWMoCuCBFe coating and its wear reduction mechanism [J]. Friction, 2022, 10: 1424−1438.

球磨时间对 TiB_2−石墨杂化增强 Cu 基复合材料显微组织演化和摩擦学性能的影响

李恒青[1]，陆均明[1]，高义民[2]，周圣丰[1]，郭柏松[1]，王怡然[2]，李 卫[1]，刘洋赈[1,2,3]

1. 暨南大学 化学与材料学院 先进耐磨蚀及功能材料研究院，广州 510632；
2. 西安交通大学 金属材料强度全国重点实验室，西安 710049；
3. 暨南大学 韶关研究院，韶关 512027

摘 要：研究球磨时间对 TiB_2−石墨杂化增强铜基复合材料显微组织和摩擦学性能的影响。采用热压烧结法制备了不同球磨时间下(4、6、8、10 和 12 h)的铜基复合材料，并对其摩擦学性能进行了研究。结果表明：复合材料的相对密度和电导率随球磨时间的延长先增加后下降；经 6 h 球磨后制备的复合材料的相对密度和电导率最高，分别为 99.1%和 42.8%(IACS)。复合材料的摩擦因数和磨损率随球磨时间的延长为先降低后增加。经 6 h 球磨后合成的复合材料的摩擦因数和磨损率最低，分别为 0.234 和 1.974×10^{-5} $mm^3/(N\cdot m)$。球磨 6 h 后制备的复合材料的主要磨损机制为磨粒磨损。

关键词：金属基复合材料；磨损机制；球磨时间；热压烧结；摩擦学性能

(Edited by Wei-ping CHEN)